Study of Al-Cu Hume-Rothery alloys and their relationship to the electronic properties of quasicrystals

1998 J. Phys.: Condens. Matter 10 4231

(http://iopscience.iop.org/0953-8984/10/19/011)

J. Phys.: Condens. Matter **10** (1998) 4231–4244. Printed in the UK PII: S0953-8984(98)85597-5

Study of Al–Cu Hume–Rothery alloys and their relationship to the electronic properties of quasicrystals

Vincent Fournée†, Esther Belin-Ferré†§ and Jean-Marie Dubois‡

† Laboratoire de Chimie Physique Matière et Rayonnement, UMR 7614 and GDR CINQ, 11 rue Pierre et Marie Curie, 75231 Paris Cédex 05, France

‡ Laboratoire de Science et Génie des Matériaux Métalliques, UMR 7584 and GDR CINQ, Ecole des Mines de Nancy, Parc de Saurupt, 54042 Nancy, France

Received 30 June 1997

Abstract. The stability of quasicrystals is related to the Hume–Rothery mechanism known to take place in many intermetallics, especially Al–Cu alloys. In order to assess to what extent the electronic density of states in aperiodic Al–Cu–Fe compounds is sensitive to Hume–Rothery stabilization, we present experimental measurements by soft x-ray emission and absorption spectroscopies of the aluminium electronic states in a series of Al–Cu crystalline compounds. Some of them, like icosahedral Al–Cu–Fe, are characterized by nearly spherical Brillouin zones. We observe the opening of a narrow but definite pseudo-gap in such Al–Cu compounds. We point out a strong interaction between Cu d states and the Al states in the middle of the valence band which is well described by a Fano-like effect. Some other characteristic features of our spectra are interpreted on the basis of band structure calculations. A comparison to previous data published for quasicrystalline and approximant phases stresses the importance for the stability of these compounds of sp–d hybridization at the Fermi level. It also leads to the conclusion that the effect of Hume–Rothery interaction is dramatically enhanced by the hierarchical structure of quasicrystals rather than by the almost spherical shape of the Brillouin zone.

1. Introduction

The electronic properties of quasicrystals have been the subject of numerous experimental and theoretical investigations due to their unusual behaviour for alloys based on good metals like fcc Al (Janot 1994, Janot and Mosseri 1995, Takeuchi and Fujiwara 1998). Their very high electrical resistivity, that furthermore increases with decreasing temperature and improved structural quality, the low carrier concentration and reduced density of states at the Fermi level, are well known features characteristic of quasicrystals (Poon 1993). The fundamental question is to understand how quasiperiodicity will affect the properties of these materials. Does the self-similarity of the structure require a new approach, different from the band-structure approach in crystals or from localization in disordered solids? Band structure calculations performed for approximant phases (Fujiwara 1989, Fujiwara and Yokokawa 1991, Hafner and Krajci 1992, 1993) are in line with the existence of the pseudo-gap observed experimentally at the Fermi level (E_F) (Belin and Traverse 1991, Belin *et al* 1992, 1994a, b, Belin-Ferré *et al* 1996). Current interpretations invoke a Hume–Rothery mechanism (HR), optimum in the case of quasicrystals because of the high multiplicity of the Bragg planes resulting from icosahedral symmetry (Friedel and Dénoyer 1987). According

§ Contact author. E-mail address: belin@ccr.jussieu.fr

0953-8984/98/194231+14$19.50

to this high multiplicity, the pseudo-Brillouin zone (hereafter for short PBZ) is closely approaching a sphere for it is a truncated polyhedron of the icosahedral group. Such a PBZ may be defined by taking into account only the most important Fourier components of the electron scattering potential in reciprocal space. Also, the average electron density turns out to be the exact density that fits the Fermi sphere into contact with the facets of the PBZ. In Al–Cu–Li, it is equal to 2.2 electrons per atom (e^-/at) whereas in Al–Cu–Fe and Al–Pd–Mn icosahedral phases it amounts to 1.85 e^-/at. It must be stressed however that this latter calculation assumes negative valences for the Fe and Mn atoms, irrespectively of their local environment. Despite that fact that this last assumption might be questionable, it is still reasonable to assign the peculiar stability of quasicrystals to the interaction between Bragg planes and electronic waves.

This view is however not entirely satisfactory, as we will see later in this paper, for conventional crystalline Al–Cu alloys, well known to be Hume–Rothery type compounds with e/a in the vicinity of 1.8 e^-/at and Brillouin zone (BZ) close to a sphere, do not exhibit the exact characteristics of quasicrystals. With this in mind, we present here several experimental results on the electronic distributions for a set of binary Al–Cu alloys, performed using soft x-ray emission and absorption. Our study was designed to determine the possible spectral characteristics induced by the HR conditions as a function of increasing isotropy of the BZ zone in order to compare quasicrystals for which the PBZ zone is almost spherical.

The first part of the paper describes the Al–Cu samples which we have studied and shows with quantitative arguments that they are of the HR type. Then, we recall the experimental methodology. The results are presented and discussed in a third part with the help of band structure calculations performed on related crystals using APW or TB–LMTO–ASA methods. Comparison with previous data obtained from the same experimental methodology eventually leads us to discuss the origin of the pseudo-gap observed in quasicrystals.

2. Samples

In this work, our aim is to analyse the effect of the HR criterion on the formation of the pseudogap observed in quasicrystalline alloys. For such a purpose, we focus our attention on the Al–Cu system for two reasons. The first one is that Al and Cu atoms have small differences in electronegativity and radii ($\Delta R_{at} < 15\%$) and that the phase diagram presents various structures for which the HR conditions might be fulfilled. Also, the BZ display a wide variety of shapes, including nearly spherical ones. The second reason is that the Cu d band lies far enough from the Fermi level (about 4 eV in these alloys) so that it will not affect the Fermi surface–Brillouin zone interaction that we are looking at.

The six alloys which we choose are listed in table 1 together with some relevant crystallographic information. The samples were prepared using 99.95% pure element for Al and Fe and 99.99% pure Cu. They were melted in an induction furnace under an argon atmosphere. Further annealing was performed to obtain single phase alloys. The characterization of the phases was achieved by using x-ray diffraction experiments.

Each of the phases has a composition very close to the boundary of its existence domain and verifies the $k_F \sim K/2$ condition, where K is the reciprocal lattice vector associated with a strong peak of the diffraction pattern. The Al content ranges from 35 to 66 at.%, scanning a large number of structures, from the simple monoclinic AlCu with 20 atoms per unit cell to the cubic γ-brass Al_4Cu_9 wit 52 atoms per unit cell. Some of the phases have CsCl-related structures of the type that are found in the Al–Cu–Fe phase diagram, neighbouring the icosahedral $Al_{62}Cu_{25.5}Fe_{12.5}$ phase (i-AlCuFe). For example, the unit cell of γ-Al_4Cu_9 can

Table 1. Crystallographic data of the alloys prepared for the present study.

Phase	Composition	Structure type	Lattice	Space group	Parameters (nm)
γ	$Al_{35}Cu_{65}$	Al_4Cu_9	cubic	$P-43m$	$a = 0.8703$
δ	$Al_{39}Cu_{61}$		rhombohedral	$R3m$	$a = 0.8789$, $\alpha = 89.78^\circ$
ζ	$Al_{43}Cu_{57}$	Al_9Cu_{12}	monoclinic	m^*21	$a = 0.707$, $b = 0.408$, $c = 1.002$, $\beta = 90.63^\circ$
η	$Al_{50}Cu_{50}$	AlCu	monoclinic	$C2/m$	$a = 1.2066$, $b = 0.4105$, $c = 0.691$, $\beta = 124.96^\circ$
ϕ	$Al_{10}Cu_{10}Fe$	Al_3Ni_2	hexagonal	$P-3m1$	$a = 0.4136$, $c = 0.509$
θ	Al_2Cu	Al_2Cu	tetragonal	$I4/mcm$	$a = 0.6063$, $c = 0.4872$

Table 2. Important reflections of the Hume–Rothery Al–Cu compounds.

Phase	Index	K (Å^{-1})	Multiplicity	Index	K (Å^{-1})	Multiplicity	$2k_F$ (Å^{-1})	e/a	N
γ	411	3.063	24	330	3.063	12	3.166	1.70	36
δ	306	3.062	8	324	3.068	4	3.178	1.78	36
	−336	3.062	4	330	3.073	2			
	5–24	3.068	4	502	3.072	4			
	630	3.073	4	−534	3.068	4			
	−552	3.072	2						
ζ	311	3.148	4	021	3.143	4	3.160	1.86	32
	−311	3.136	4	005	3.135	2			
	204	3.090	2	114	3.083	4			
	020	3.080	2	310	3.079	4			
	−114	3.067	4	−204	3.058	2			
η	−313	3.127	4	−511	3.103	4	3.232	2.00	24
	020	3.061	2	−512	3.046	4			
	112	3.046	4	311	3.103	4			
	202	3.125	2						
ϕ	110	3.037	2	012	3.028	8	3.050	1.81	18
	−210	3.037	4	1–12	3.037	4			
θ	310	3.274	8	202	3.305	8	3.334	2.33	16

be viewed as $3 \times 3 \times 3$ distorted CsCl cubes, with formula unit $Al_{16}Cu_{36}V_2$ (V is a vacancy site). The structural relationship between these vacancy ordered CsCl-related phases and quasicrystalline i-AlCuFe has been pointed out by Dong (1996). The $Al_{10}Cu_{10}Fe$ phase with Al_3Ni_2 structure and the Al_9Cu_{12} compound with a modified γ-brass structure (Dong 1995) are of peculiar interest as they lie very close to the line with constant electron per atom ratio $e/a = 1.85$ in the AlCuFe system, along which the icosahedral phase forms (Dong *et al* 1994).

For each alloy, we have determined the shape of the BZ defined as the polyhedron constructed from the bisecting planes associated with reciprocal vectors K with a non-vanishing structure factor and satisfying the HR condition $k_F \sim K/2$. The radius of the FS, k_F, is given in the free electron model by the relation $k_F \sim (3\pi^2 n)^{1/3}$, where the electronic density n is calculated using the valences $+3$, $+1$ and -2 for Al, Cu and Fe, respectively. Table 2 gives the values of $2k_F$ for the different alloys as well as the reciprocal lattice vectors K from which the BZ is constructed, the corresponding multiplicity, e/a and the number of contact points N between the Fermi surface (FS) and the BZ. The way we have defined N is specified hereafter. In each case, the corresponding x-ray diffraction peaks are the most intense of the diffraction pattern.

The electronic stabilization of a system depends on several factors. The strength of the Fourier component V_K of the potential seen by the electrons and the multiplicity of the corresponding Bragg planes determine the width and the depth of the pseudo-gap. The potential V_K can be written as the product

$$V_K = S(K)V_{ps}(K) \tag{1}$$

where $S(K)$ is the structure factor $S(K) = N^{-1}\sum_R \mathrm{e}^{\mathrm{i}KR}$ and $V_{ps}(K)$ is the pseudopotential at point K of the reciprocal lattice. The pseudopotential for copper is about six times larger than that for aluminium at the Fermi level, so the Cu atoms scatter predominantly both the valence electrons and x-rays (Cohen and Heine 1970). It is then reasonable to conclude that an intense Bragg peak will be associated with a strong V_K (Friedel and Dénoyer 1987). Furthermore, we verified on a set of our samples that the Bragg peaks of the x-ray diffraction patterns from which the BZ are constructed give rise also to strong diffraction by fast electron scattering. In such an experiment, the Fourier transform of the Coulomb potential is obtained whereas an x-ray diffraction experiment gives the Fourier transform of the corresponding electronic density, both being connected by the Poisson relation.

There is also a 'closeness condition' between $2k_F$ and K which states that the band contribution to the total energy will be minimized if the FS just comes into contact with the BZ boundaries. To see whether or not a Bragg plane should be included in the BZ, we need an estimation of the interval ΔK in the reciprocal space where the electronic states are perturbed. In a free electron model, ΔK is related to V_K by

$$\left(\frac{\mathrm{d}}{\mathrm{d}k}E(k)\right)_{(k_F)} = h v_F = \frac{2V_K}{\Delta K} \tag{2}$$

where v_F is the Fermi velocity. Assuming a value of 0.5 eV for V_K, which is usual for Al based alloys (Ashcroft 1979), we find a value of $\Delta K \cong 0.1$ Å^{-1}. This condition is fulfilled in our alloys as it is in i-AlCuFe for example.

As a conclusion, we have verified that our alloys are all indeed Hume–Rothery compounds, some of them being rather good candidates to study the spectral features induced by this genuine effect alone.

3. Experimental techniques

In order to investigate the electronic distributions, we have used the soft x-ray-emission and soft-x-ray-absorption spectroscopies (SXES and SXAS) which provide separately information on the valence and conduction bands (VB and CB respectively). Let us recall the principles of these methods. In SXES, the sample is irradiated with electrons of sufficient energy to create a hole in an inner level. One of the decay processes is the emission of a photon accompanying an electron transition from the VB to the core hole. The energy distribution of the emitted photons is proportional to the density of states (DOS) in the VB and to the radiative transition probability W between the initial state of wave function ψ_i (which describes a hole in the inner level) and the final state of wave function ψ_f (which describes a hole in the VB). The probability W is a function of the square of the dipolar matrix element $\langle\psi_i|\varepsilon r|\psi_f\rangle$. So the x-ray emission is submitted to the dipolar selection rules ($\Delta l = \pm 1$, $\Delta j = 0, \pm 1$) and depends on the overlap of the highly localized state ψ_i with the rather extended one ψ_f. Consequently, in an alloy, SXES gives the local electronic distributions for each type of atom with a given symmetry.

In SXAS, the energy of an incident photon is absorbed by a core electron which is ejected into the conduction band. The absorption spectrum describes the sum of all the

transitions towards the continuum levels of the appropriate symmetry. Experimentally, one measures the current associated with the electrons escaped from the sample owing to photoabsorption. If I_0 is the intensity of the incident photon beam and I the intensity at a depth x in the sample, the fraction of the intensity absorbed is

$$(I_0 - I)/I_0 = \gamma(1 - \mathrm{e}^{-\mu x}) \cong \gamma \mu x = Y \tag{3}$$

where γ is a constant, μ is the linear attenuation coefficient and Y the photoyield. The coefficient μ is a function of the photoabsorption cross section $\bar{\omega}$ of the different elements. The variation of $\bar{\omega}$ is given by

$$\Delta\bar{\omega} = h\nu|\langle\psi_i|\Sigma r_i|\psi_f\rangle|^2\rho_f(\nu = \nu_{fi}) \tag{4}$$

where ψ_i and ψ_f are the wave functions describing, in the one-electron approximation, the inner electron and the electron ejected in the conduction state, respectively, r_i is the position of the ith core electron and ρ_f is the DOS of the CB. Here again, the transition is required to obey the dipolar selection rules and depends on the overlap of an extended state with a highly localized one. This makes the SXAS site and symmetry selective. Consequently, SXAS as well as SXES can be used as local and partial probes of the electronic structure when applied to a multicomponent system.

The SXES (SXAS) spectra are the convolution product of the valence DOS (conduction DOS) with the Lorentzian energy distribution of the core level, weighted by the transition probability. The energy distribution of this probability is usually negligible over the width of a band so that the spectra are directly related to the corresponding DOSs. Thus, we can compare the shape of the different partial distributions in various alloys but no absolute DOS values can be derived from the experiments. All the spectral curves presented in this paper are normalized to their maximum intensity.

For a meaningful discussion of the electronic interactions in the solid, it is worthwhile to adjust all the partial distribution curves in the unique binding energy scale, with the Fermi energy E_F as the origin. This is made possible using XPS measurements of the binding energies of the inner levels involved in the probed x-ray transitions (Belin and Traverse 1991, Belin *et al* 1992).

The SXES measurements were carried out with Johann-type vacuum spectrometers fitted with either a grating 600 grooves mm^{-1} bent with a radius of 2 m or with $SiO_2(10\bar{1}0)$ or Beryl$(10\bar{1}0)$ crystals bent with a radius of 0.5 m. Al CB states were probed at the synchrotron facility of LURE (Orsay, France) using the Super-ACO storage ring at the SA 32 beam line fitted with a two-quartz crystal monochromator. The width of the core level is usually the most important limitation to the resolution of the SXS techniques. The values are given in table 3 for the analysed transitions (Krause and Oliver 1979). The energy range of the recorded spectra, the analyser used and the final energy resolution are also reported.

Table 3. Analysed x-ray transition, probed states and energy range, analyser used, resolution and width of the inner level involved in the x-ray transitions.

X-ray transition	Probed states	Energy range (eV)	Analyser	Resolution (eV)	Width of the inner level (eV)
OB → Al 1s	Al 3p	1550–1565	$SiO_2(10\bar{1}0)$	0.2	0.42
OB → Al $2p_{3/2}$	Al 3s–d	55–85	grating	0.2	<0.1
OB → Cu $2p_{3/2}$	Cu 3d	920–940	Beryl	0.3	0.56
Al 1s → UB	Al p	1555–1585	SiO_2	0.2	0.42

The Cu $2p_{3/2}$ and Al $2p_{3/2}$ binding energies have been obtained with a spectrometer fitted with an Al anode as the x-ray source and calibrated using the binding energy of the C contamination 1s level energy taken equal to 285.0 eV. The value for the Al 1s level could not be obtained directly. It was deduced from complementary measurements of the Al Kα_1 ($2p_{3/2} \rightarrow$ 1s) line. Within the experimental precision, the wavelength of the Al Kα_1 line is the same in pure Al and in the alloys. Finally, we could locate E_F on the transition scales within $\pm$0.2 eV for Al and $\pm$0.3 eV for Cu.

4. Results and discussion

The Cu Lα spectral curves (3d–4s $\rightarrow$ $2p_{3/2}$) shown in figure 1 reflect essentially the occupied 3d distribution because the probability of a d–p transition is much higher than that of an s–p one and, in addition, the contribution of the s states to the occupied band is already faint in elemental Cu (Papaconstantopoulos 1986). In all samples, the Cu 3d distributions have almost the same shape as in pure Cu. The maximum lies at about 4 eV from E_F so that it is shifted towards the centre of the VB as compared to the pure metal. The position of the peak varies from 3.4 ± 0.3 eV to 4.1 ± 0.3 eV according to the Cu concentration and local environment (Fournée *et al* 1998). The structures observed on the low binding energy (BE) side of the curves labelled α', α''' and α'' on the curve for Al_2Cu are satellite emissions. However, if we define the principal part of the spectral distribution as the high BE part of the Lα curve plus its symmetric, the actual full width at half maximum intensity

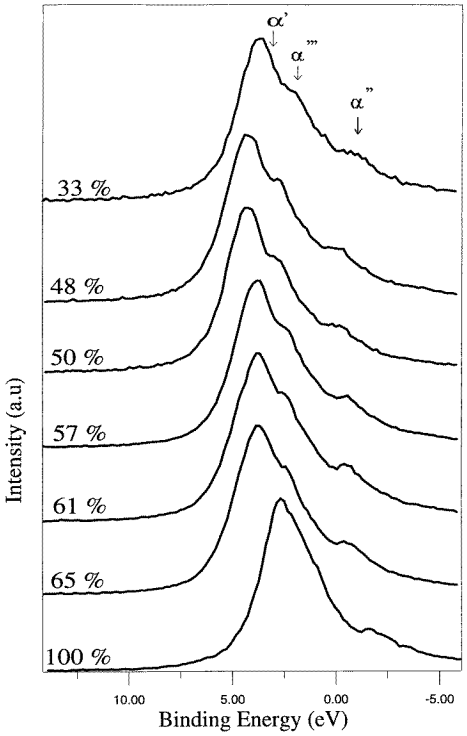

Figure 1. Cu Lα emission band of Cu metal and of the Al–Cu Hume–Rothery alloys. Cu concentration increases from top to bottom.

(FWHM) of the Cu Lα band becomes 2.85 eV in the pure element and about 2.6 eV in the alloys. This small narrowing is due to an alloying effect, the Cu–Cu coordination number being reduced in the alloys with respect to the pure metal.

Let us recall that in pure Al (inset of figure 2), a typical free-electron system, the distributions are parabolic-like, with a narrow peak near E_F for the partial 3s–d contribution. This peak arises from (i) the infrared catastrophy, due to the generation of electron–hole pairs of very low energy accompanying the creation of the core hole in a nearly-free-electron system (Nozières and de Dominicis 1969) and (ii) the presence near E_F of states with some d character (Papaconstantopoulos 1986, Léonard 1978). The Al 3p and 3s–d distributions overlap on the entire VB; consequently the states are sp hybridized, with some d character close to E_F. Figure 2 shows the Al 3s–d distribution curves in the alloys. The shape of these distributions are significantly modified as compared to the pure metal, consistently with what one can expect for extended states. The 3s–d DOS is greatly enhanced in the 5–10 eV BE region and reduced in the lower BE region over about 4 eV from E_F, so that the bottom of the Al 3s–d band has an almost pure s character. Its maximum lies between 6 and 7 eV from E_F and its minimum is around 4 eV, close to the position of the Cu d maximum. This asymmetric deformation is a common feature observed in transition metal–simple metal alloys. It is related to the Fano effect as discussed by Terakura (1977). The interaction between the relatively narrow d band and the broad sp bands results in

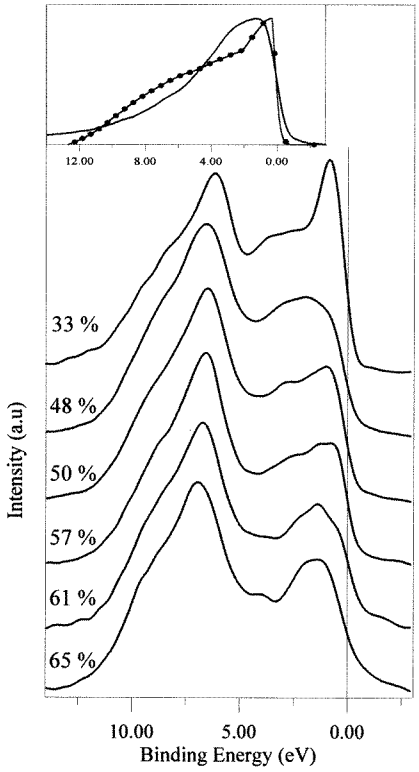

Figure 2. Al s–d distribution curves in the Al–Cu Hume–Rothery alloys. Cu concentration increases from top to bottom. The inset shows the Al 3s–d and 3p distribution curves for pure Al.

the formation of a hybridization gap which splits the simple metal sp states into bonding and antibonding parts. For concentrated alloys, the position of the d resonance does not necessarily coincide with the antiresonance dip, denoted AR hereafter (i.e. the minimum in the hybridization gap), whereas it is practically the case in the impurity limit described by the Anderson model (Anderson 1961). In our Al–Cu alloys, the position of the minimum in the Al 3s–d distribution follows approximately the shift of the Cu d maximum with the Cu concentration. With respect to the AR dip position, the shift of the Al 3s bonding peak, $\Delta\sigma$, is a function of the hybridization matrix element between Al s and Cu d states. It increases as the Cu concentration increases from 2.0 ± 0.2 eV in the θ phase (33 at.% Cu) to 3.3 ± 0.2 eV in the γ phase (65 at.% Cu), as reported in figure 3. Note that some Al states of d character remain near E_F which are responsible for the structure observed between $+1$ and $+2$ eV in the spectra. This point is discussed in a forthcoming paper (Fournée *et al* 1998).

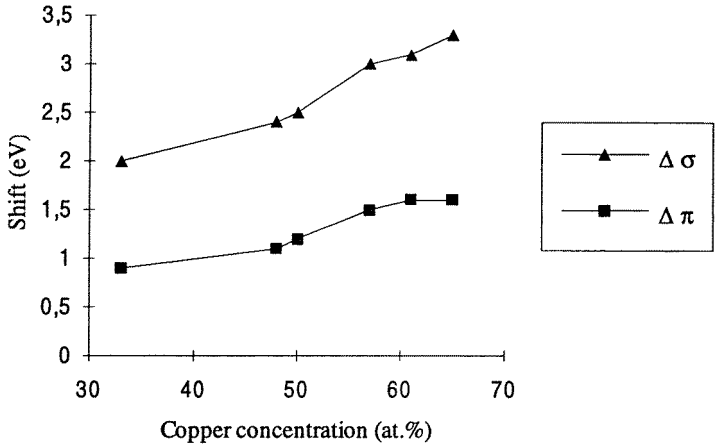

Figure 3. Shift of the Al s and Al p bonding peaks with respect to the antiresonance dip position.

The coupling between the Al p and Cu d states results also in the splitting of the Al 3p distribution. The two parts are located on each side of the Cu d band with the AR dip at about 4 eV (figure 4). The shift of the maximum of the bonding peak with respect to the AR dip position, $\Delta\pi$, increases with the Cu concentration, from 0.9 ± 0.2 eV in the θ phase 1.6 ± 0.2 eV in the γ phase (figure 3). As far as the Al 3p edge is concerned, it is repelled from E_F by about 0.3 eV at half the maximum intensity as compared to pure Al. This makes the intensity of the corresponding Al Kβ spectral curve at the Fermi level reduce to 40% of the maximum intensity or less in the alloys, against 50% in pure fcc Al.

The interpretation of the experimental features based on the work of Terakura (1977) has been confirmed by a set of band structure calculations on hypothetical Al–Cu alloys using the APW method. More details about these calculations will be given elsewhere (Fournée *et al* 1998). As an example, figures 5(a) and 5(b) show the calculated Al $L_{2,3}$ and Al Kβ spectra for an equiatomic AlCu compound in the CsCl structure. As recalled in the previous section, the experimental spectral distribution curves reflect the product $|M|^2 N(E) \times L(E)$ where M is the matrix element of the x-ray transition probability, $N(E)$ is the partial DOS and $L(E)$ is a Lorentzian function whose FWHM is the energy width of the inner level involved in the x-ray transition. Thus, for a meaningful comparison with the experimental spectra, we have broadened each partial DOS by a convenient $L(E)$ and,

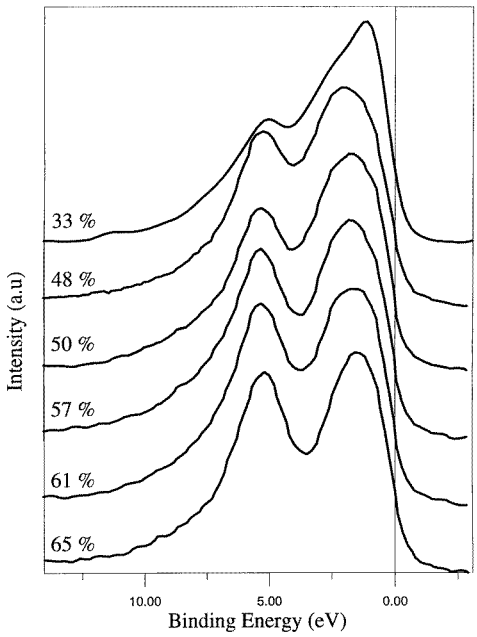

Figure 4. Al p distribution curves in the Hume–Rothery alloys. Cu concentration increases from top to bottom.

to account for the instrumental function of the spectrometer, we have smoothed the result by a Gaussian function G. The widths of $L(E)$ and G functions are given in table 3. The Al $L_{2,3}$ calculated curve contains the Al s DOS plus two-fifths of the Al d DOS. The factor $2/5$ arises directly from the selection rules that allow transitions for which $\Delta m = \pm 1$ or 0. On average, only $2/5$ of the d states can make a transition to a p state (Goodings and Harris 1969). We neglected the variation of the transition matrix element over the width of the band. We find the same features as in the experimental distribution curves: the positions of the peaks are in good agreement, the splitting of the Al p states into bonding and antibonding parts is well reproduced and the Al s states are repelled by the interaction with the Cu d states. The hybridization gap is clearly seen in the Al s and p LDOS. Al d states are present around 5 eV from E_F; they are hybridized to the Al p and Cu d states and could be responsible for the faint structure observed in several of the Al $L_{2,3}$ spectra within the same energy range (see for example Al $L_{2,3}$ curve of the γ phase). Note however that there is a discrepancy concerning the relative peak intensities of the Al Kβ and Al $L_{2,3}$ calculated spectra when compared to the experimental ones. For equivalent compositions, the intensity of the bonding peak seems to be overestimated in the calculations as compared to the experimental results (Fournée *et al* 1998).

The intensity of the Al p conduction band at the Fermi level is adjusted assuming that the distribution of p character is a continuous function of the energy. This assumption is valid if the transition probabilities W between the Al 1s wave function ψ_i and either the wave function ψ_f describing the Al 3p valence state or the Al p conduction state can be considered as nearly equal. As mentioned in the first part, W depends on the overlap between ψ_i and ψ_f. Only the amplitude of ψ_f in the region of the Al core contributes to the transition matrix element. As shown in figure 6, the conduction band is slightly flattened as compared to that of pure Al, but less than in approximant and quasicrystalline phases (Belin-Ferrré and Dubois 1996).

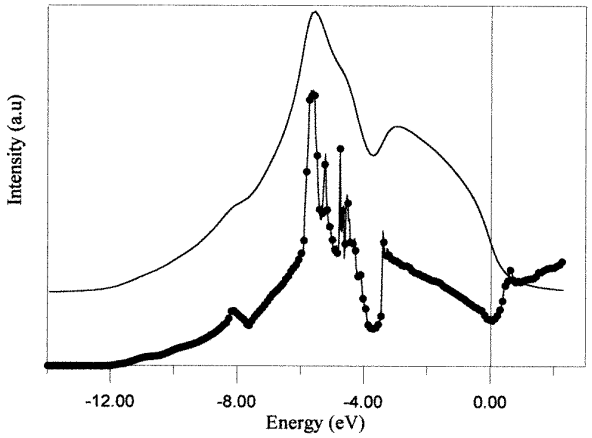

(a)

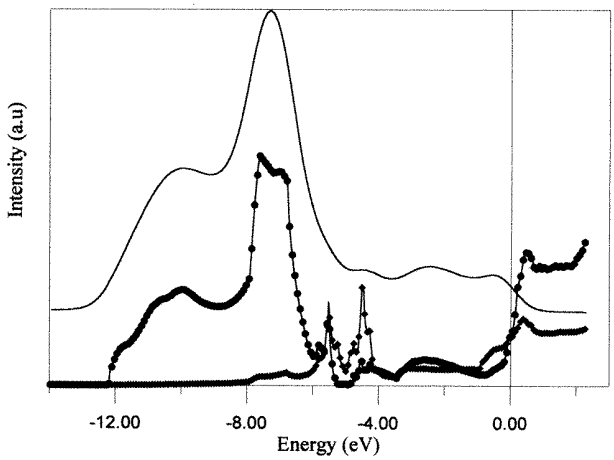

(b)

Figure 5. (a) Al p DOS (dotted line) and the corresponding calculated Al Kβ spectrum (full line) for a model AlCu alloy in CsCl-type structure. (b) Al s (dotted line) and Al d (line with squares) DOS and corresponding calculated Al $L_{2,3}$ spectra (full line) for a model AlCu alloy in CsCl structure.

As mentioned, the Al 3p distribution in the alloys is repelled from E_F and the intensity of the corresponding Al Kβ spectra at the Fermi level is reduced in the alloys with respect to the pure metal. Thus, a small pseudo-gap is observed experimentally in the distribution of Al p states at the Fermi level which can be assigned to both the sp–d hybridization and the diffraction by the Bragg planes. The depletion should increase with the number of contact points between the Fermi surface and the Brillouin zone. However, the differences observed in the XES spectra from one alloy to the other are small. This might be due to the fact that the broadening of the DOS by the Lorentzian distribution of the inner level and the experimental resolution hide this effect which concerns a small energy region around E_F scaling with V_K.

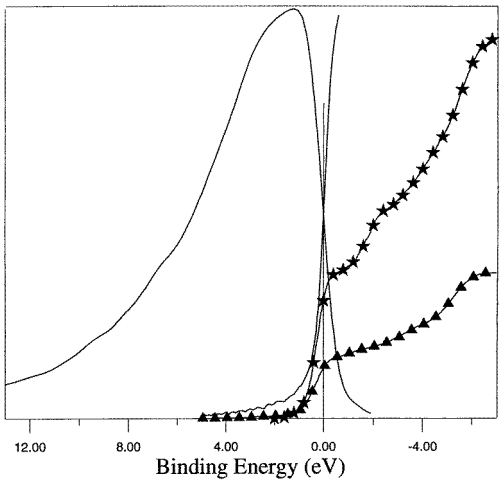

Figure 6. Al p CB distribution curves in pure Al (full line), γ-$Al_{35}Cu_{65}$ (starred line) and i-AlCuFe (line with triangles) alloys as adjusted to the Al 3p intensity at the Fermi level (see text). For clarity only the Al 3p distribution curve of pure Al is shown.

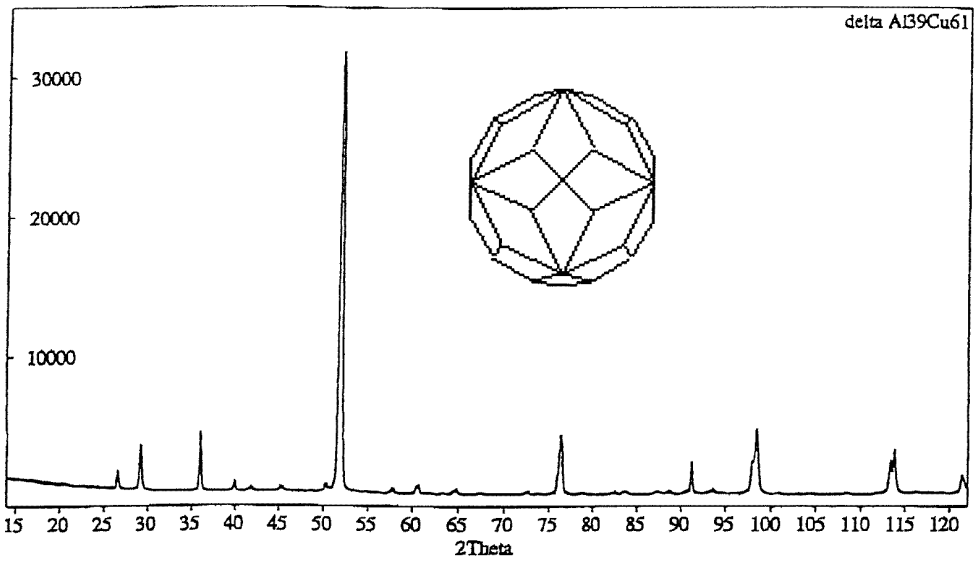

Figure 7. X-ray diffraction pattern of the δ-$Al_{39}Cu_{61}$ phase and its Brillouin–Jones zone.

Our alloys are HR compounds and consequently a pseudo-gap is expected at E_F. The one we observe is quite small as compared to the pseudo-gap in approximant and quasicrystalline alloys, where I_F goes down to less than 15% in icosahedral phases. Nevertheless, the FS–BZ interaction should be strong, especially in the case of the γ and δ phases, where the BZ is constructed with 36 faces corresponding to Bragg peaks that concentrate almost all the intensity of the x-ray diffraction pattern as shown in figure 7. The partial Al p DOS in γ-Al_4Cu_9 calculated using the TB–LMTO–ASA method and the corresponding calculated Al Kβ spectra are presented in figure 8. In that case, a direct

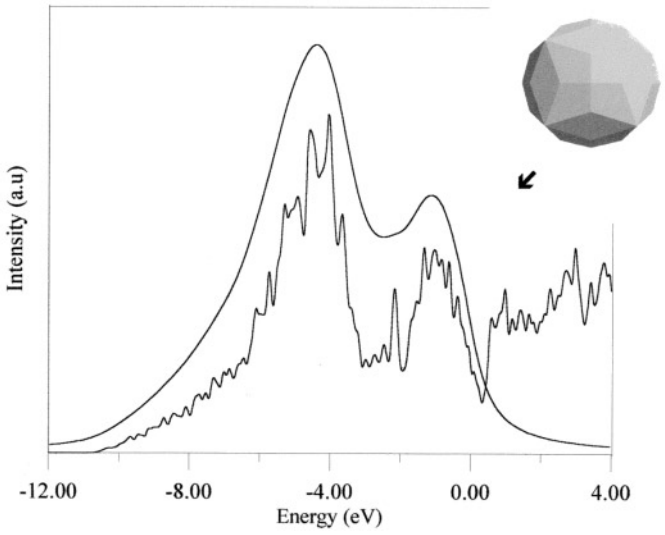

Figure 8. Experimental (top) and calculated (bottom) Al p DOS curves of the γ-Al_4Cu_9 phase and its Brillouin zone.

comparison with γ-$Al_{35}Cu_{65}$ is possible, as it has the same γ-brass structure. The Fermi level falls in a pronounced pseudo-gap, confirming the strong FS–BZ interaction. The width of this pseudogap is about 1 eV. After broadening, the relative intensity at E_F is $I_F = 40\%$, just as the experimental value. Taking the number of faces N as a rough parameter for the sphericity of the BZ, the comparison with the case of the approximant $Al_{13}Fe_4$ or the quasicrystalline i-AlCuFe, with N equal to 30 and 42 respectively, shows that the HR mechanism alone is not sufficient to explain the formation of the pseudogap observed by SXS in Al–TM–TM′ quasicrystalline phases (TM, TM′: transition metals). The wider depletion cannot be the result of a more spherical shape of the PBZ, differences with the γ phase being too small.

More likely, the effect of the TM should be invoked. Indeed, it has been shown (Friedel 1992, Trambly de Laissardière *et al* 1995) that the presence of TM d states of energies close to the gap, coupled to the sp states, results in an increase of the magnitude of the potential acting on the Fermi electrons and consequently an increase of the width of the resulting pseudo-gap. Previous experiments on Al–TM alloys have revealed indeed the strong Al p–TM d hybridization at E_F, the result of which is to repel the electronic states on both sides of the Fermi level, giving rise to an enhanced pseudo-gap (Belin *et al* 1992, 1994a, Belin-Ferré *et al* 1996). The p–d hybridization is even responsible for the opening of an almost true gap in Al_2Ru and Ga_2Ru semiconductors (Nguyen Manh *et al* 1992, Fournée *et al* 1997). Note that these two effects, diffraction by Bragg planes and hybridization with TM d states, should not be considered as distinct effects as the sublattice of the TM atoms contributes predominantly to the scattering potential V_K. Note also that the HR effect has almost no influence on the flattening of the Al p CB within the normalization scheme exposed above. This is consistent with the conclusion of Belin-Ferré and Dubois (1996) who noticed the continuous change in the shape of the Al p CB, from a $\tan^{-1}(E)$ behaviour to a parabolic-like one when going from pure Al to perfect i-AlCuFe. Such a dependence of the DOS in the CB is in good accordance with the

model proposed by Janot and de Boissieu (1994) and Janot (1995). In this model, the structure is described by a hierarchical self-similar packing of atomic clusters, named pseudo-Mackay icosahedra (PMIs). These basic units combine to reproduce a similar configuration via an inflation operation with a scale factor close to τ^3 giving rise to a cluster of PMI clusters. The structure develops via successive steps of this inflation process (Janot 1997). The PMIs are supposed to be very stable and, in a simple jellium model, they behave as a spherical well confining most of the electrons on the cluster levels. Then the valence band consists in the bonding states of the elementary PMI plus the bonding states of the clusters in the next steps of the inflation process. The special electron per atom ratio arises from the constraint for PMIs at each stage of the hierarchy to have a closed electronic shell to ensure stability of the system. All the occupied states are bonding states and the conduction states are then free states, thus showing an $E^{1/2}$ dependence.

5. Conclusion

With the aim to examine the possible influence of the HR factor on the formation of the pseudo-gap as observed by SXS in quasicrystalline phases, we have studied Al–Cu alloys of the HR type. This allowed us to separate the contributions of the two related factors that participate in the gap opening in sp–d quasicrystals: scattering by Bragg planes and presence of TM d states at E_F. The interaction between the Cu d states and the electronic states of Al that takes place at about 4 eV from E_F appeared to be Fano type. Our results show that the FS–BZ interaction in Al–Cu crystals gives rise to a sizeable effect, somewhat smeared out by the broadening effects inherent to the SXS techniques. Hence, the differences observed with increasing isotropy of the BZ are very small. Comparison with similar studies on crystalline, approximant or quasicrystalline phases stresses the importance of the sp–d hybridization at E_F by increasing the width and the depth of the pseudogap and making it easier to observe by spectroscopic measurements.

Acknowledgments

We are grateful to Z Dankhazi, P Donnadieu, A M Flank, P Lagarde, I Mazin, D A Papaconstantopoulos, A Sadoc and M Zandona for their collaboration in experiments and assistance in calculations. The hospitality offered to VF by the Naval Research Laboratory (Washington, DC, USA) and to VF and EB-F by the Institute for Experimental Physics at the Technical University of Vienna (Austria) is warmly acknowledged. This work has been supported in part by the Austrian Ministry of Research, East–West Cooperation program under the title ‘Soft x-ray spectroscopy of metallic systems’.

References

Anderson P W 1961 *Phys. Rev.* B **124** 41
Ashcroft N W 1979 *Phys. Rev.* B **19** 4906
Belin E, Dankhazi Z and Sadoc A 1994a *Mater. Sci. Eng.* A **181/182** 717
Belin E, Dankhazi Z, Sadoc A, Calvayrac Y, Klein T and Dubois J M 1992 *J. Phys.: Condens. Matter* **4** 4459
Belin E, Dankhazi Z, Sadoc A and Dubois J M 1994b *J. Phys.: Condens. Matter* **6** 8771
Belin E and Traverse A 1991 *J. Phys.: Condens. Matter* **3** 2157
Belin-Ferré E, Dankhazi Z, Sadoc A, Berger C, Müller H and Kirchmayr H 1996 *J. Phys.: Condens. Matter* **8** 3513
Belin-Ferré E and Dubois J M 1996 *J. Phys.: Condens. Matter* **8** L717

Cohen M L and Heine V 1979 *Solid State Physics* vol 24 (New York: Academic) p 37
Dong C 1995 *J. Physique* I **5** 1625
——1996 *Phil. Mag.* A **73** 1519
Dong C, Perrot A, Dubois J M and Belin E 1994 *Mater. Sci. Forum* **150/151** 403
Fournée V, Belin-Ferré E, Dubois J M, Mazin I and Papaconstantopoulos D A 1998 *Phil. Mag.* B submitted
Fournée V, Belin-Ferré E, Trambly de Laissardière G, Sadoc A, Volkov P and Poon S J 1997 *J. Phys.: Condens. Matter* **9** 7999
Friedel J 1992 *Phil. Mag.* B **6** 1125
Friedel J and Dénoyer F 1987 *C. R. Acad Sci., Paris* II **305** 171
Fujiwara T 1992 *Phys. Rev.* B **40** 942
Fujiwara T and Yokokawa T 1991 *Phys. Rev. Lett.* **66** 333
Goodings D A and Harrs R 1969 *J. Phys. C: Solid State Phys.* **2** 1808
Hafner J and Krajci M 1992 *Phys. Rev. Lett.* **68** 2321
——1993 *Phys. Rev.* B **47** 11 795
Janot C 1994 *Quasicrystals: a Primer* 2nd edn (Oxford: Oxford University Press)
——1995 *Phys. Rev.* B **5** 181
——1997 *J. Phys.: Condens. Matter* **9** 1493
Janot C and de Boissieu M 1994 *Phys. Rev. Lett.* **72** 1674
Janot C and Mosseri R (eds) 1995 *Proc. 5th Int. Conf. on Quasicrystals, ICQ5* (Singapore: World Scientific)
Krause M O and Oliver J H 1979 *J. Phys. Chem. Data.* **8** 329
Léonard P 1978 *J. Phys. F: Met. Phys.* **8** 467
Nguyen Manh D, Tramby de Laissardière G, Julien J P, Mayou D and Cyrot-Lackmann F 1992 *Solid State Commun.* **82** 329
Nozières P and de Dominicis C T 1969 *Phys. Rev.* **178** 6105
Papaconstantopoulos D A 1986 *Handbook of the Band Structures of Elemental Solids* (New York: Plenum)
Poon J S 1993 *Adv. Phys.* **41** 303
Takeuchi R and Fujiwara T (eds) 1998 *Proc. 6th Int. Conf. on Quasicrystals, ICQ6* (Singapore: World Scientific) at press
Terakura K 1977 *J. Phys. F: Met. Phys.* **7** 1773
Trambly de Laissardière G, Nguyen Manh D, Magaud L, Julien J P, Cyrot-Lackmann F and Mayou D 1995 *Phys. Rev.* B **52** 7920